RESEARCH

Influence of the Size and Dielectric Environments on the Optical Properties in CdS/ZnS Core–Shell Quantum Dot

Naima Yahayaoui[1] · Nabil Zeiri[1] · Pınar Baser[2] · Moncef Said[1] · Salah Saadaoui[3]

Abstract

In this work, the electronic and optical properties of CdS/ZnS core–shell quantum dots (CSQDs) capped in different matrices were investigated theoretically. Through the effective mass approximation (EMA) and the density matrix approach (DMA), the quantized energy levels and their corresponding wave functions of the system were obtained by solving the Schrödinger equation in a spherical coordinates system. In addition, the effects of the incident optical intensity, the number of dots per unit volume, dielectric mismatch of the organic and inorganic matrix, and geometric parameters of the structure, such as the core/shell radius ratio for CdS/ZnS CSQDs on the optical properties, were evaluated and discussed. The results revealed that both the size and dielectric environments had a substantial effect on the optical features of these nanostructures.

Keywords Intersubband transition · Nonlinear optics · Dielectric environment · Maxwell–Garnett (MG) formalism

Introduction

CSQDs have aroused a great challenge in the last few years thanks to their particular roles in potential technological applications in many fields including optoelectronics and biology [1, 2]. Recently, theoretical and experimental studies have reported that encapsulating CSQDs into an appropriate matrix material deal with new optical properties [3–8]. Indeed, surrounding the CSQD with Hafnium dioxide (HfO_2), polyvinyl alcohol (PVA), polyvinyl chloride (PVC), or silicon dioxide (SiO_2) is usually required [9, 10] to insure the QD stabilization and enhances new optical properties. Zaiping et al. [11] have investigated the third-order nonlinear optical absorption coefficient (AC) in colloidal CdS QDs capped by various dielectric matrices. Their computational study revealed that the QD capped by a matrix material having the largest energy band gap exhibits the largest threshold

energy. Employing a variational approach, Niculescu [12] considered the effect of the surrounding medium intending to conclude about the variation of the donor binding energy in CdSe/ZnTe CSQDs. They deduced that neglecting the effect of dielectric mismatch in calculations inevitably leads to erroneous scientific outcomes. Moreover, in Anchala Purohit and Mathur [13], Anchala et al. evaluated the effect of the dielectric environment on the third-order nonlinear optical susceptibility $\chi^{(3)}$. Their findings revealed that the refractive index change (RIC) and peaks corresponding to AC are blue-shifted when the barrier height due to the capping matrix raises. In 2012, Cristea and Niculescu [14] used the EMA to examine the electronic properties of CdSe/ZnS and ZnS/CdSe CSQDs embedded in large-gap dielectric materials. Their results indicated that the aimed energy range for the impurity levels could be adjusted within these dielectrically modulated nanostructures. The authors in [15] have studied how dependent the dielectric function (DF), susceptibility, RI, and AC of the slab are on the geometric factor and density of the QDs-matrix. They mentioned that when the volume fraction climbs, the contribution of high-frequency dielectric constant increases while the offset of RI tends to the high-frequency dielectric constant of the dots. In Hemdana et al. [16], reporters have numerically investigated the influence of the MEH-PPV matrix on the optical properties of a spherical CdSe/ZnS

✉ Nabil Zeiri
zeirinabil@gmail.com

1 Laboratory of Condensed Matter and Nanosciences (LMCN), Department of Physics, Faculty of Sciences of Monastir, 5019 Monastir, Tunisia

2 Sivas Cumhuriyet University Turkey, Sivas, Turkey

3 Department of Physics, Faculty of Science and Arts, King Khalid University, Mohayel Aser, Abha, Saudi Arabia

CSQD. They found that in CdSe/ZnS capped in MEH-PPV organic matrix, the radiative lifetime is higher than that in CdSe/ZnS CSQDs. In Holmström et al. [10], investigated the complex DF of QDs within a core–shell structure in tetrachloroethylene (TCE) medium. Assuming the EMA and the MG formalism, they concluded that they could obtain the accurate polarizability for the particle in the long-wavelength limit by a homogenized dielectric function for CSQDs.

The goal of this work is to explore numerically the impact of the dielectric mismatch of CdS/ZnS c/s nanostructure on the linear, the third-order nonlinear DF, and the effective DF. Under the EMA, the energy levels and their corresponding wave functions are computed numerically by solving the Schrödinger equation in spherical coordinates. The theoretical explorations are presented based on these numerical calculations as follows. The "Theory and Computational Details" section deals with the description of our theoretical background. Our numerical results and related discussions are given in the "Results and Discussion" section. Finally, the "Conclusion" section is dedicated to the major conclusions.

Theory and Computational Details

Our adopted model consists of a confined single electron in CdS/ZnS CSQDs, R_c designates the internal radius corresponding to CdS (core), whereas R_s designates the external radius corresponding to ZnS (shell) and the whole structure is encapsulated in a dielectric material. The potential discrepancy between materials pictorially represents a barrier and a well and the detailed geometry of the CSQDs-matrix is illustrated in Fig. 1.

As the band gap of the core (CdS) is narrower than that of the shell (ZnS), the core material potential was chosen as the zero-reference energy, thus $V_{0e} > 0$ [17].

By using the E M A and in a two parabolic bands model, the one particle Hamiltonian expressed in spherical coordinates is given by:

$$\left(-\frac{\hbar^2}{2m_j^*}\Delta + V(r) + W(r) \right)\Psi_{n,l,m}(r,\theta,\varphi) = E\Psi_{n,l,m}(r,\theta,\varphi)$$

(1)

where m_j^* is the effective mass of the electron in QD, $V(r)$ is the confinement potential, which is the sum of the potential

Fig. 1 Schematic diagram of the confinement potential of CdS/ZnS CSQDs encapsulated in various matrices: SiO$_2$, PVC, or PVA
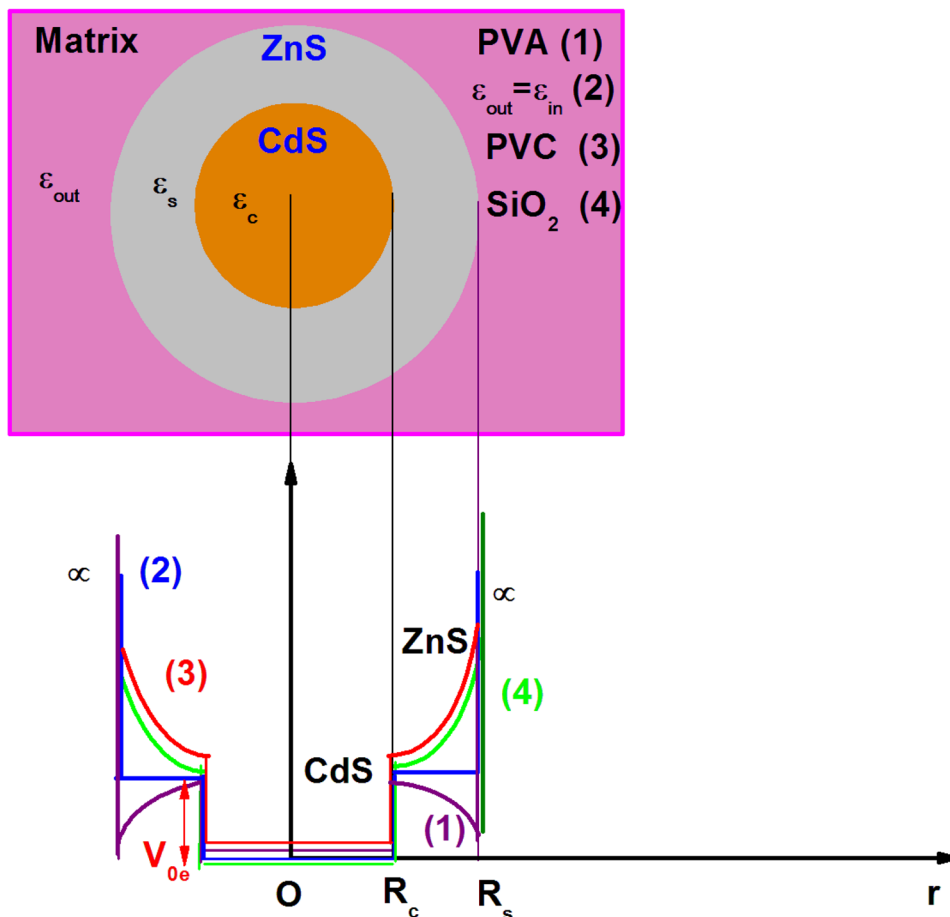
due to the band discontinuity between the CdS/ZnS materials, and $W(r)$ the self-polarization energy correction is given by [11, 18]:

$$W(r) = \frac{e^2(\varepsilon_{in} - \varepsilon_{out})}{8\pi R_S \varepsilon_{in}} \sum_{k=0}^{\infty} \frac{k+1}{k\varepsilon_{in} + (k+1)\varepsilon_{out}} \left(\frac{r}{R_s}\right)^{2k} \quad (2)$$

The effective masses are expressed as:

$$m_j^* = \begin{cases} m_{CdS}^* & r < R_1 \\ m_{ZnS}^* & R_1 < r \leq R_2 \end{cases} \quad (3)$$

And the barrier potential in the heterostructure is expressed as:

$$V(r) = \begin{cases} 0, & 0 < r \leq R_1 \\ V_{0e} & R_1 < r \leq R_2 \\ \infty & r > R_2 \end{cases} \quad (4)$$

where ε_{in} and ε_{out} are the permittivity of the nano-spherical layer and the medium respectively.

By considering the solution of Eq. (1) as:

$$\psi_{n,l,m}(r, \theta, \varphi) = R_{nl}(r).Y_{l,m}(\theta, \varphi) \quad (5)$$

To calculate $R_{nl}(r)$, two cases need to be distinguished: $E > V_c$ and $E < V_c$. We have followed the theoretical formalism described in Zeiri et al. [17].

And the following equation incarnates the normalization's condition [17]:

$$(R_i(r) = R_{i+1}(r))_{r=r_i} \quad (6)$$

$$\left(\frac{1}{m_i^*}\frac{dR_i(r)}{dr} = \frac{1}{m_{i+1}^*}\frac{dR_{i+1}(r)}{dr}\right)_{r=r_i} \quad (7)$$

And

$$\int_0^{\infty} |R_i(r)|^2 dr = 1 \quad (8)$$

Hamiltonian from Eq. (1) is a sum of two operators: H_0 and $W(r)$. After computing the energy levels and their corresponding wave functions for the operator H_0, we will use $W(r)$ as an additional term to calculate the change of energy according to first-order perturbation theory. Change in the energy of (ΔE) can be calculated as [19]:

$$\Delta E = \int_0^{R_c} R_{nl}(r)W(r)R_{nl}(r)r^2 dr + \int_{R_c}^{R_s} R_{nl}(r)W(r)R_{nl}(r)r^2 dr \quad (9)$$

ΔE depends on the behavior of $R_{nl}(r)$ and $W(r)$. However, the energy of an electron confined in CSQD nanostructure can be expressed as $E = E_0 + \Delta E$

Furthermore, assimilating our system to two energy levels, the fundamental and the first excited states, in this framework, the linear and the third-order nonlinear optical susceptibilities are given by [17, 20]:

$$\chi^{(1)}(\omega) = \frac{\sigma_v |M_{21}|^2}{(E_{21} - \hbar\omega - i\hbar\Gamma)} \quad (10)$$

$$\chi^{(3)}(\omega) = \frac{\sigma_v |M_{21}|^2}{E_{21} - \hbar\omega - i\hbar\Gamma} \left[\frac{4|M_{21}|^2}{(E_{21} - \hbar\omega)^2 + (\hbar\Gamma_{12})^2} - \frac{(M_{22} - M_{11})^2}{(E_{21} - i\hbar\Gamma_{12})(E_{21} - \hbar\omega - i\hbar\Gamma_{12})} \right] \quad (11)$$

where σ_v represents the carrier density, $\Delta E_{ij} = E_i - E_j$ the inter-level energy transition between the ground and excited states, $M_{ij} = F|\langle \Psi_i | er | \Psi_j \rangle|$ donates the electric dipole moment, and F is the local electric factor given by: $F = \frac{3\varepsilon_{out}}{\varepsilon_{int} + 2\varepsilon_{out}}$.

Then, the analytical form of the linear and nonlinear DF of the CSQDs structure is given by [20]:

$$\varepsilon^{(1)}(\omega) = 1 + 4\pi\chi^{(1)}(\omega) \quad (12)$$

$$\varepsilon^{(3)}(\omega) = 4\pi\chi^{(3)}(\omega) \quad (13)$$

The total dielectric function $\varepsilon(\omega, I)$ of CSQDs is expressed as follows:

$$\varepsilon(\omega, I) = \varepsilon^{(1)}(\omega) + |E|^2\varepsilon^{(3)}(\omega) = 1 + 4\pi \frac{\sigma_v |M_{21}|^2}{(E_{21} - \hbar\omega - i\hbar\Gamma)}$$

$$-4\pi \frac{|E|^2 \sigma_v |M_{21}|^2}{(E_{21} - \hbar\omega - i\hbar\Gamma)} \left[\frac{4|M_{21}|^2}{(E_{21} - \hbar\omega)^2 + (\hbar\Gamma_{12})^2} - \frac{(M_{22} - M_{11})^2}{(E_{21} - i\hbar\Gamma_{12})(E_{21} - \hbar\omega - i\hbar\Gamma_{12})} \right] \quad (14)$$

For CdS/ZnS spherical core/shell QD, the explicit equation giving the effective DF is given by [20]:

$$\varepsilon_{eff}(\omega) = 1 + 3p + 9p$$
$$\left\{ 3 + 4\pi \frac{\sigma_v |M_{21}|^2}{(E_{21} - \hbar\omega - i\hbar\Gamma)} - 4\pi \frac{|E|^2 \sigma_v |M_{21}|^2}{(E_{21} - \hbar\omega - i\hbar\Gamma)} \left[\frac{4|M_{21}|^2}{(E_{21} - \hbar\omega)^2 + (\hbar\Gamma_{12})^2} - \frac{(M_{22} - M_{11})^2}{(E_{21} - i\hbar\Gamma_{12})(E_{21} - \hbar\omega - i\hbar\Gamma_{12})} \right] \right\}^{-1} \quad (15)$$

where p represents the volume concentration of the dots defined as $p = \frac{4\pi R^3}{3} n$. And n is the number of dots per unit volume.

However, the effective DF is adopted within the framework of the Maxwell-Garnet formalism, as reported in Vahdani [20, 21].

Results and Discussion

In this survey, the numerical calculations were performed to analyze the electronic, linear, and third-order nonlinear DF, and the effective DF of CdS/ZnS CSQDs capped in a dielectric matrix were calculated.

The schematic representation of the spherical core/shell QDs is depicted in Fig. 1 and the structural parameters adopted in modeling are picked from Zeiri et al. [17]: $m^*_{e,CdS} = 0.18$ m_0, $m^*_{e,ZnS} = 0.42$ m_0, and $V_{0e} = 0.897$ eV. Furthermore, we

have neglected, for simplicity, the effect of lattice mismatch between the core/shell materials and embedding matrix in our numerical calculations. For this reason, we assumed $\varepsilon_{in} = \sqrt{\varepsilon_{r(CdS)} \cdot \varepsilon_{r(ZnS)}} = 8.9$ [22] and when the CSQDs is embedded in different matrix with different dielectric constants $\varepsilon_{out} = 3.9$, 4.8, and 14 for SiO_2, PVC and PVA respectively [23, 24].

In Fig. 2, we have displayed the fluctuations of the ground state energy E_1 and the first excited state E_2 with core-to-shell radii ratio R_c/R_s of an uncovered CdS/ZnS core/shell nanostructure (Fig. 2c) and for a CSQDs surrounded by three different dielectric matrices symbolized SiO_2 (Fig. 2a), PVC (Fig. 2b), or PVA (Fig. 2d) matrix respectively. It is observed from this figure that the presence of a dielectric medium is strongly influenced the electron energies. Indeed, for a small ratio, the slight increase in energies is attributed to the dielectric constants of the embedding. Physically, in the case of CSQDs immersed in an organic or inorganic matrix, additional
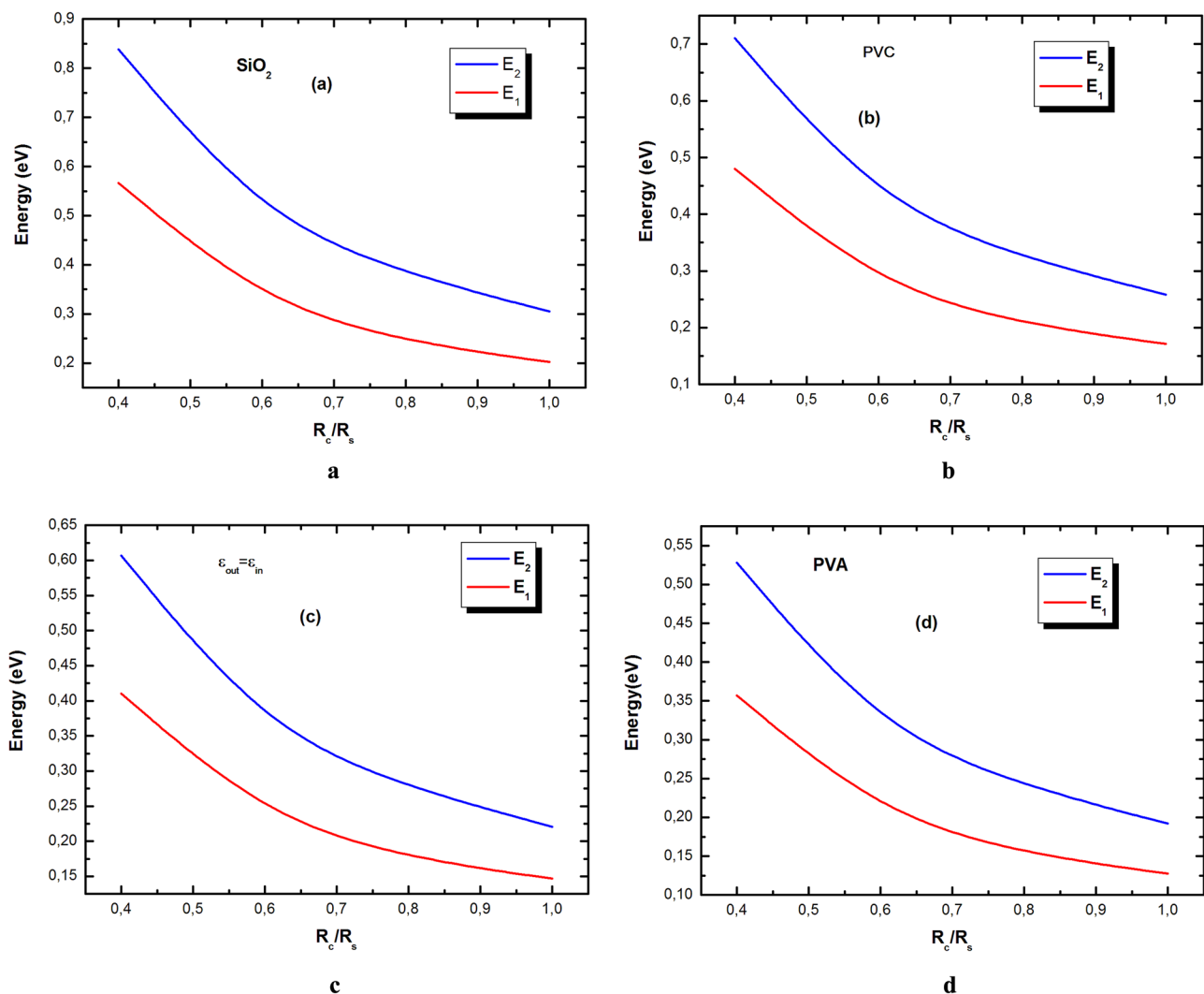
Fig. 2 The variation of the energy levels of electrons E_1 and E_2 as a function of the core/shell radii ratio R_c/R_s encapsulated by SiO_2 **a**, PVC **b**, and PVA **d** respectively and for an isolated CSQDs **c**

self-interaction energy will appear. This is due to the interaction of the charge with its own induced charges. The discontinuity of the dielectric constant between the semiconductor and the dielectric environment affects the electron energy states. Additionally, as the ratio R_c/R_s increases, the electron energy decreases rapidly and tends to the continuum. This is due to the quantum confinement effect. The dielectric mismatch and geometrical parameters are two factors that need to be taken into consideration especially in CSQDs when probing novel optical properties. These conclusions have been reported in the literature [9–14].

To compute the electronic and optical properties of the optoelectronic devices, the intersubband transition energy ΔE_{12} must be managed as precisely as possible and the influence of the dielectric environment such as organic or inorganic medium must be explicitly understood. In Fig. 3, we have plotted the change of the ΔE_{12} as a function of R_c/R_s for the proposed matrix SiO$_2$, PVC, PVA, and isolated CSQDs ($\varepsilon_{out}=\varepsilon_{in}$). As expected, the plot confirms that ΔE_{12} is significantly affected by the dielectric matrix. According to our calculations, for $R_c/R_s=0.6$, the transition energy ΔE_{12} for each dielectric matrix is ΔE_{12} (PVA)$=0.114$ eV, ΔE_{12} (PVC)$=0.155$ eV, and ΔE_{12} (SiO$_2$)$=0.183$ eV. A difference can be observed when the CSQDs structure is not capped in any dielectric matrix ($\Delta E_{12}=0.113$ eV). Our results reflect that the performance of optoelectronic devices can be handled by combining the effect of variation in dimensions and a suitable dielectric environment. This result is due to the influence of the dielectric environment which modifies the electronic structure of the CSQDs [8, 10].

The Real $\varepsilon(\omega, I)$ and Im $\varepsilon(\omega, I)$ versus photon energy $\hbar\omega$ are plotted in Fig. 4 in the presence of various dielectric environments: SiO$_2$, PVC, and PVA in the case of $\varepsilon_{out}=\varepsilon_{in}$ for $E < V_c$ under the condition of $I=0.2$ MW/cm^2 and $R_c/R_s=0.6$. From the plot, as can be seen that, the intensity and location of the resonance peaks corresponding to the CSQDs embedded in a dielectric medium are different from those of isolated CSQDs ($\varepsilon_{out}=\varepsilon_{in}$). Our study highlights the effect of the surrounding matrix and that it should not be ignored in the calculations. The presence of a dielectric medium such as organic or inorganic materials induces superficial charges at the boundaries. These induced charges interact in turn with the particles which will affect the electron spectrum. From this figure, it is readily seen that the $Real\varepsilon(\omega, I)$ reaches the maximum in the case of the PVA matrix and change significantly its sign from -2.0 to $+2.0$ near the resonance photon energy 0.115 eV while the peak value of $Im\varepsilon(\omega, I)$ is 3.086. On the other hand, by choosing the SiO$_2$ matrix, the $Real\varepsilon(\omega, I)$ switches from -1.4 to $+1.4$ near the resonance 0.174 eV while the $Im\varepsilon(\omega, I)$ has reached the value 1.84. We can say that a higher dielectric constant (case of SiO$_2$) exhibits a large amplitude of computed coefficients. Immersing CSQDs in a dielectric medium can give a blue or red shift with the size modulated by the magnitude of optical properties. This conclusion has been deduced by many researchers [9, 14].

In order to test the effect of the capped matrix on the DF, we turn our attention to the influence of the light intensity on the Real $\varepsilon(\omega, I)$ and Im $\varepsilon(\omega, I)$ in the case of

Fig. 3 The inter-level transition ΔE_{12} variation as a function of the core/shell radii ratio R_c/R_s for the CdS/ZnS core–shell structure in the presence of various dielectric matrices: SiO$_2$, PVC, and PVA
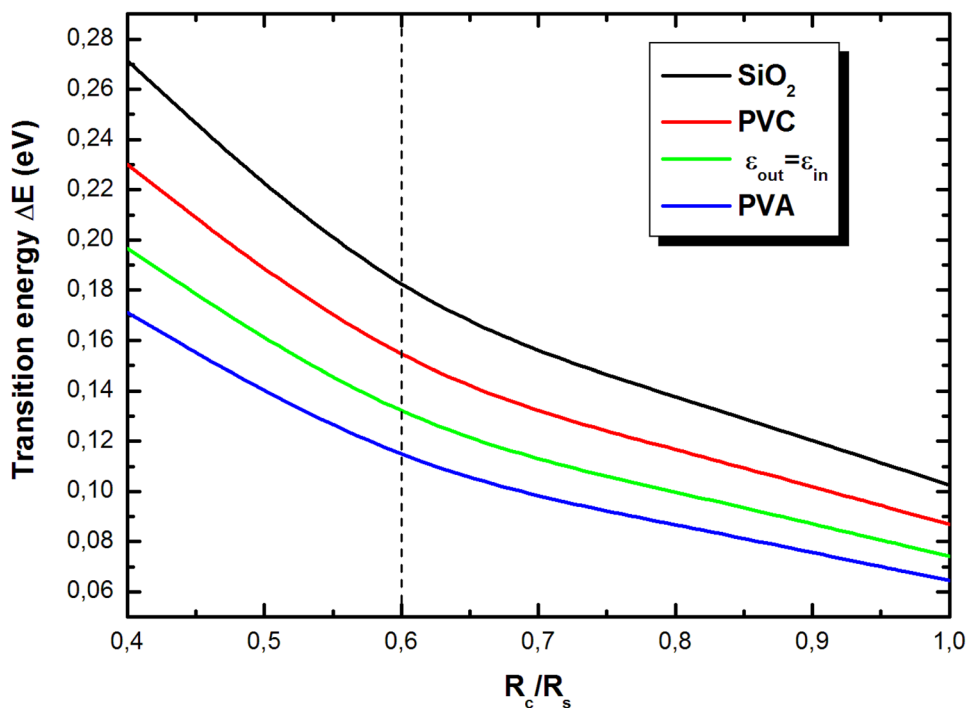
Fig. 4 The real and imaginary parts of the permittivity $\varepsilon(\omega, I)$ with $\hbar\omega$ (eV) in the presence of various dielectric matrices: SiO_2, PVC, and PVA under the condition of $n = 3.10^{-16}$ cm^{-1}, $I = 0.2$ MW/cm^2, and $R_c/R_s = 0.6$
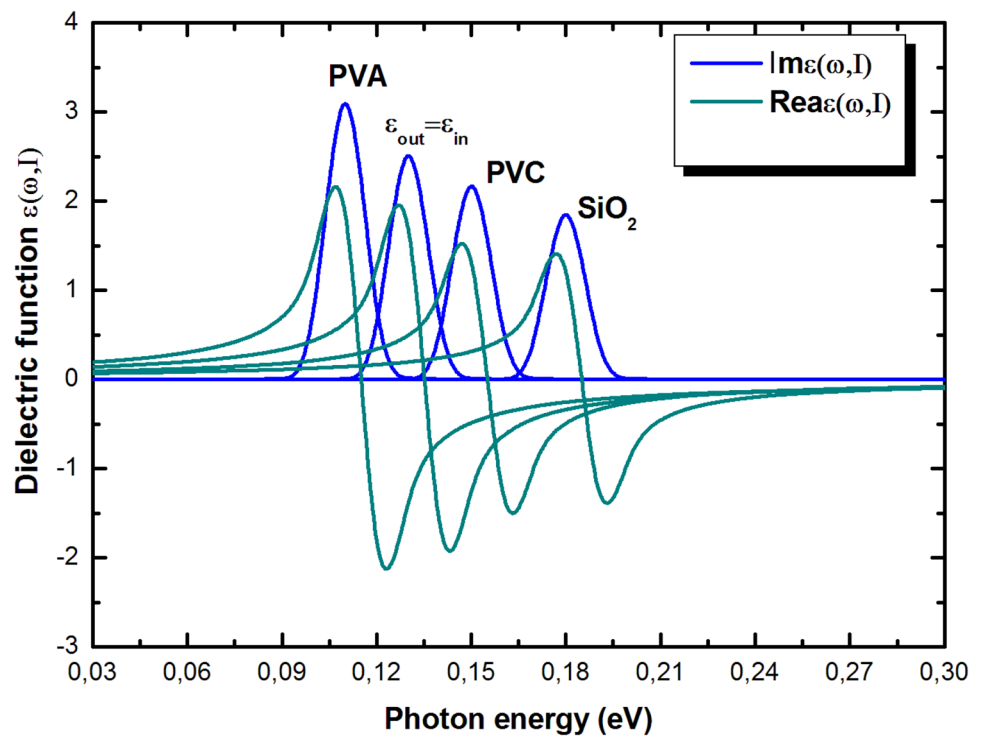

the PVA matrix for a fixed value radii ratio $R_c/R_s = 0.6$ (Figs. 5 and 6). From the plot, as can be seen, Real $\varepsilon(\omega, I)$ and Im $\varepsilon(\omega, I)$ are strongly affected by the optical intensity I. It is found that the magnitude of both the Real $\varepsilon(\omega, I)$ and Im $\varepsilon(\omega, I)$ decreases with increasing I. This reduction is due to the nonlinear contribution which decreased

the amplitude of the imaginary and real parts of the total permittivity $\varepsilon(\omega, I)$. Our results are similar to those of the reference [14].

In order to explore in detail the impact of the dielectric mismatch at the CSQD-matrix boundary, we have depicted in Fig. 7, the $Real\varepsilon_{eff}$ and $Im\varepsilon_{eff}$ with $\hbar\omega$ (eV) in the presence

Fig. 5 The imaginary part of the permittivity $\varepsilon(\omega, I)$ with $\hbar\omega$ (eV) for the matrix PVA with different values of the optical intensity I under the condition of $n = 3.10^{-16}$ cm^{-1} and $R_c/R_s = 0.6$
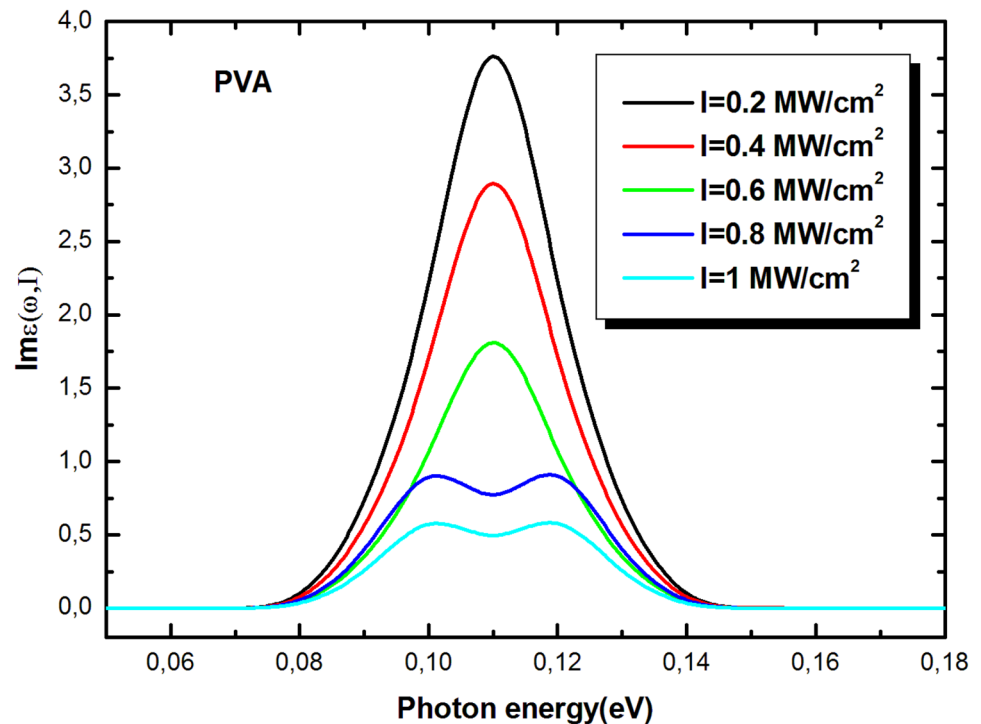
Fig. 6 The real part of permittivity $\varepsilon(\omega, I)$ with $\hbar\omega$ (eV) for the matrix PVA with different values of optical intensity with $n = 3.10^{-16}$ cm^{-1} for $R_c/R_s = 0.6$
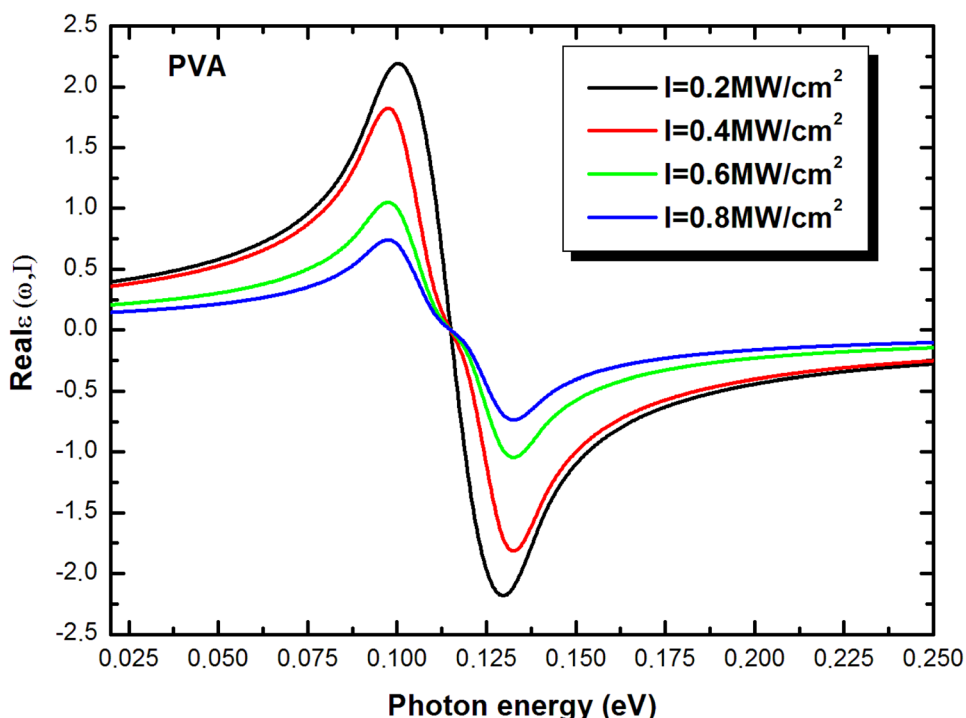

of various dielectric environments: SiO$_2$, PVC, and PVA in the case $E < V_c$ with a fixed value of core-to-shell radii ratio $R_c/R_s = 0.6$. By analyzing the figure, we can remark that the magnitude of the $Real\varepsilon_{eff}$ and $Im\varepsilon_{eff}$ of CdS/ZnS CSQDs immersed by different matrices is 0.24 and 0.13

respectively. We note that the imaginary and real parts of ε_{eff} exhibit a red shift or a blue shift compared to $\varepsilon_{out} = \varepsilon_{in}$. This shift is due to the capped matrix which has dielectric constants different from those of QD materials. It can be seen that the $Real\varepsilon_{eff}$ and $Im\varepsilon_{eff}$ increase and their resonance

Fig. 7 The variation of $Im\varepsilon_{eff}$ and $Real\varepsilon_{eff}$ with $\hbar\omega$ (eV) in the presence of various dielectric environments, under the condition of $I = 0.2$ MW/cm^2, $n = 3.10^{16}$ cm^{-1}, and $R_c/R_s = 0.6$
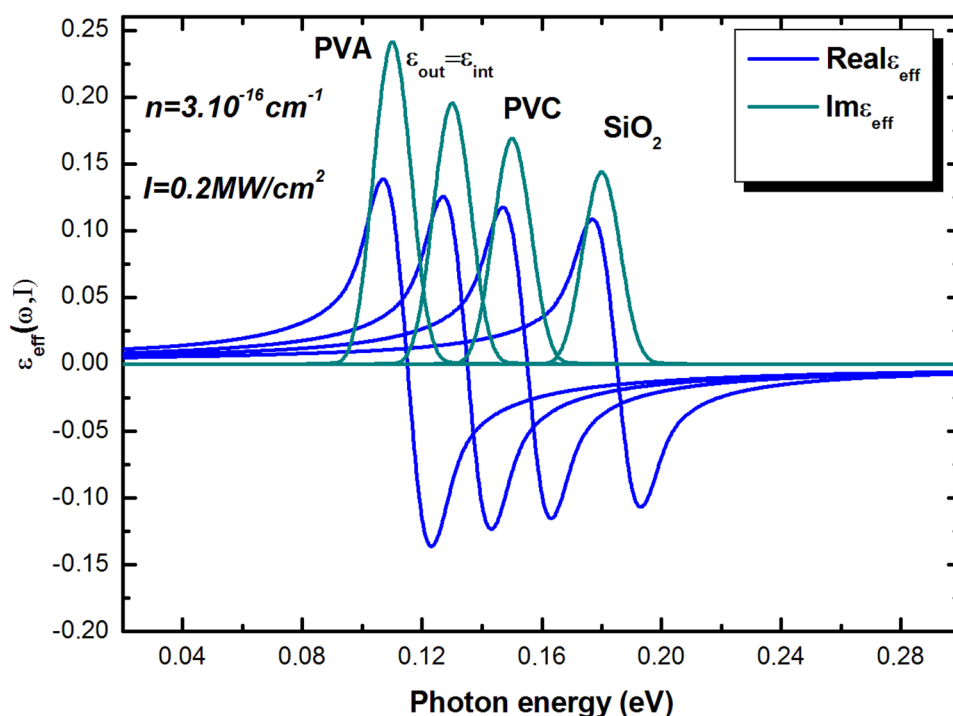
Fig. 8 The variation of $Im\varepsilon_{eff}$ with $\hbar\omega$ (eV) with different values of n, for the PVA matrix, $R_c/R_s = 0.6$ and $I = 0.2$ MW/cm.^{2}
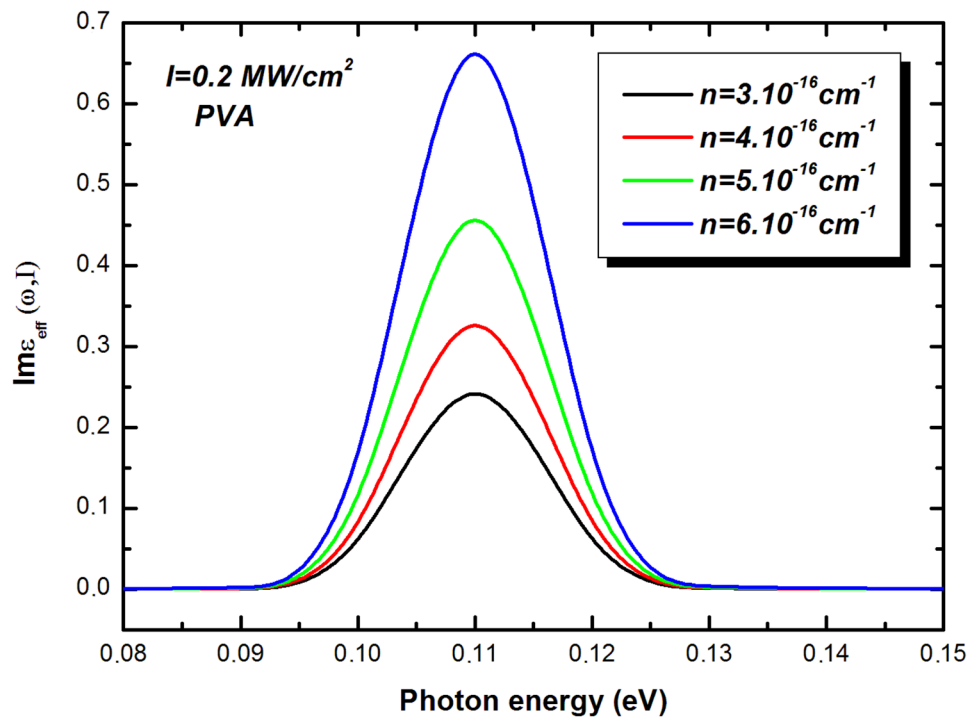
peak intensities shift to lower energy in the case of QDs/PVA, in this case $\varepsilon_{out} > \varepsilon_{in}$, the local field factor $F > 1$ which induces an increase in the transition matrix element $M_{i,j}$ and giving a stronger $Real\varepsilon_{eff}$ and $Im\varepsilon_{eff}$ magnitude results in a better overlap between wave functions. Otherwise, when $\varepsilon_{out} < \varepsilon_{in}$, in the case of SiO$_2$ and PVC matrix, the dipole

matrix element $M_{i,j}$ decreases and generates a lower magnitude. This conclusion has been mentioned in [25].

In order to improve the performance of the optoelectronic device, we have selected the appropriate matrix which gives better results ($\varepsilon_{out} = 14$).

Fig. 9 The variation of $Im\varepsilon_{eff}$ with $\hbar\omega$ (eV) for four different values of relaxation times under the condition of $n = 3.10^{-16}$ cm^{-1} and $R_c/R_s = 0.6$ for the PVA matrix
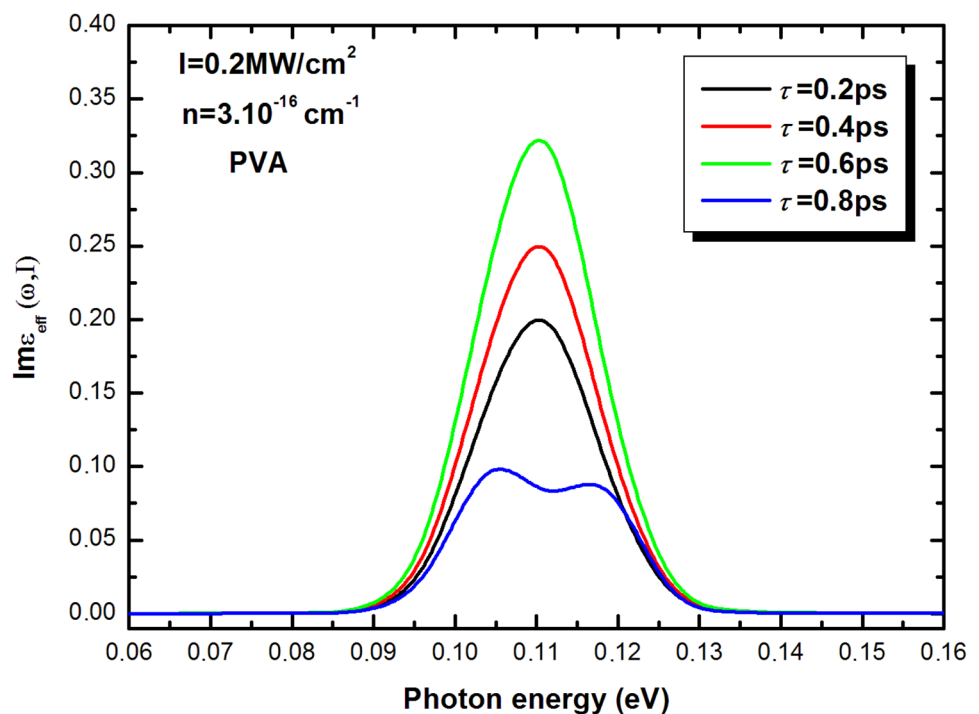
Figure 8 illustrates the variation of $Im\varepsilon_{eff}$ with $\hbar\omega$ (eV) in the case of the PVA matrix with a fixed value of core-to-shell radii ratio $R_c/R_s = 0.6$, for different values of the number density of QDs n (3, 4, 5, and 6×10^{-16} cm^{-1}) under the condition of $I = 0.2$ MW/cm^2. From this figure, we can clearly see that when n increases the magnitude of ε_{eff} increase significantly from 0.25 for $n = 3.10^{16}$ cm^{-1} to 0.65 for $n = 6.10^{16}$ cm^{-1}. The same behavior has been reported by Vahdani et al. [26]. The Im ε_{eff} depends on the optical intensity plays a key role in ultra-fast optical signal processing. It can result in many important physical processes, such as ultra-short laser pulse, optical phase conjugation, self-focusing, and self-trapping [27, 28].

Figure 9 illustrates the variation of $Im\varepsilon_{eff}$ with $\hbar\omega$ (eV) for a fixed value of n and optical intensity I in the case of the PVA matrix. The theoretical investigation includes four different values of relaxation times. From the curve, as can be seen that, there is an improvement of the $Im\varepsilon_{eff}$ magnitude when the relaxation time increases. Moreover, it is observed that when $Im\varepsilon_{eff}$ saturation occurs, the total optical DF will reduce with increasing the relaxation time. Indeed, for a higher value of τ, the imaginary parts of the effective DF peak split two peaks and were strongly bleached. Many authors have reported in their theoretical and experimental investigations that QD encapsulated in a dielectric medium can absorb and re-emit wavelengths in a more precise way which will contribute to the development of optoelectronic nano-devices [29–31].

Conclusion

In summary, we have theoretically studied the influences of the geometric parameter, optical intensity, and dielectric mismatch on the effective permittivity and optical permittivity of CdS/ZnS CSQDs encapsulated in different dielectric matrices. Our calculations revealed that the transition energy is affected by the dielectric environment. Therefore, the dielectric discontinuity at CSQD/matrix boundary should be taken into account in our computations. This investigation allows one to select the appropriate dielectric environment that provides the larger optical nonlinearities making the covered CSQDs a promising candidate for the realization of tunable nonlinear optical devices.

Data Availability We don't want to share your data before we have thoroughly analyzed it. All data sources described in this study are led by the corresponding authors.

Declarations

Ethical Approval The authors, a signatory below, declare by the present statement that all the exhibited results in this work could be very useful in the design of optoelectronic and electro-optic devices. This work opens perspectives in nanostructures field research for further advances in optoelectronics research.

Competing Interests The authors declare no competing interests.

References

1. Huang X, Tong X, Wang Z (2020) J Electron Sci Technol 100018–100029
2. Rana M, Jain A, Rani V, Chowdhury P (2019) Inorg Chem Commun 112:107723–107752
3. Elamathi M, John Peter A, Lee CW (2020) Eur Phys J D 74(10):196–214
4. Vasileiadis M, Koutselas I, Pispas S, Vainos NA (2015) J Polym Sci, Part B: Polym Phys 54(5):552–560
5. Lesyuk R, Cai B, Reuter U, Gaponik N, Popovych D, Lesnyak V (2017) Small Methods 1(9):1700189–1700199
6. Talbi A, El Haouari M, Nouneh K, Mustapha Feddi E, Addou M (2021) Eur Phys J Appl Phys 93:10401–10411
7. Onyeaju MC, Onate CA (2021) European Physical Journal D 75:1–8
8. Ibral A, Zouitine A, Assaid EM, Feddi EM, Dujardin F (2014) Physica B 449:261–268
9. Maikhuri D, Purohit SP, Mathur KC (2012) AIP Adv 2:012160–012171
10. Holmström P, Thylén L, Bratkovsky A (2010) J Appl Phys 107(6) (2010)
11. Zaiping Z, Christos S, Garoufalis S, Baskoutas S (2016) J Nanoelectron Optoelectron (11):1–5
12. Niculescu EC (2012) Superlattices Microstruct 51:814–824
13. Anchala Purohit SP, Mathur KC (2011) J Appl Phys 110:114320–114326
14. Cristea M, Niculescu EC (2012) European Physical Journal B 85(191):363–376
15. Vahdani MRK, Ehsanfard N (2018) Physica B 548:1–9
16. Hemdana I, Mahdouani M, Bourguiga R (2013) Transp Theory Stat Phys 42(6–7):381–398.064307–064313
17. Zeiri N, Naifar A, Abdi-Ben Nasrallah S, Said M (2018) Optik 176:162–167
18. Talbi A, El Haouari M, Nouneh K, Pérez LM, Tiutiunnyk A, Laroze D, Courel M, Mora-Ramos ME, Feddi E (2021) Appl Phys A 127:30(1)–30(17)
19. Stojanović D, Kostić R (2018) Opt Quant Electron 50:174(2)–174(10).
20. Vahdani MRK (2014) Superlattices Microstruct 76:326–338
21. Zeng XC, Bergman DJ, Hui PM, Stroud D (1988) Phys Rev B 38:10970–10973
22. Zeiri N, Naifar A, Abdi-Ben Nasrallah S, Said M (2020) Chem Phys Lett 744:137215–137221
23. Hewa-Kasakarage NN, El-Khoury PZ, Schmall N, Kirsanova M, Nemchinov A, Tarnovsky AN, Zamkov AM (2009) Appl Phys Lett 94(13):133113–133117
24. Zeng Z, Paspalakis E, Garoufalis CS, Terzis AF, Baskoutas S (2013) J Appl Phys 113:0543030
25. Vahdani MRK (2014) Superlattices and Microstructures 76:326–338
26. Negi CMS, Gupta SK, Kumar D, Kumar J (2013) Superlattices Microstruct 60:462–474

27. Hosseini SM, Vahedi A (2017) Optik - International Journal for Light and Electron Optics 130:1222–1228
28. Sundheep R, Prasanth R (2016) J Mater Sci: Mater Electron 28(4):3168–3174
29. Jeong H, Shin SK (2018) Chem Phys Lett 692:333–339
30. Thuy UTD, Liem NQ, Thanh DX, Protière M, Reiss P (2007) Appl Phys Lett 91(24):241908–241912
31. Casas Espínola JL, Hernández Contreras XA (2017) J Mater Sci: Mater Electron 28(10):7132–7138